

Charged basal stacking fault (BSF) scattering in nitride semiconductors

Aniruddha Konar,^{1,2, a)} Tian Fang,^{3,2} Nan Sun,¹ and Debdeep Jena^{3,2}

¹⁾Department of Physics, University of Notre Dame, Notre Dame, USA 46556

²⁾Midwest Institute of Nanoelectronics Discovery (MIND), Notre Dame, USA 46556

³⁾Department of Electrical Engineering, University of Notre Dame, Notre Dame, USA 46556

(Dated: 28 May 2022)

A theory of charge transport in semiconductors in the presence of basal stacking faults is developed. It is shown that the presence of basal stacking faults leads to anisotropy in carrier transport. The theory is applied to carrier transport in non-polar GaN films consisting of a large number BSFs, and the result is compared with experimental data.

The III-V nitride semiconductors and related compounds have attracted immense attention for optoelectronic devices^{1,2} covering a wide range of the electromagnetic spectrum as well as high-speed, high temperature electronic devices. For c-plane grown nitrides, built-in polarization field, although advantageous for two dimensional electron gas (2DEG) formation in transistors³, reduces the overlap of electron-hole wavefunction, reducing the oscillator strength for radiative transitions. Moreover, c-plane based enhancement mode transistors suffer from low threshold voltages⁴ ($V_{th} \sim 1$ V) impeding their applications in safe circuit operation. A potential way to eliminate these effects is to grow nitrides in non-polar directions. However, heteroepitaxial, non polar and semi-polar nitrides films grown on lattice mismatched substrates contain $n_{SF} \sim 1-10 \times 10^5/\text{cm}$ basal stacking faults (BSFs) parallel to the [0001] direction⁵⁻⁷. Directionally dependent transport measurements in highly faulted non-polar nitride films show strong mobility anisotropy for both electron and hole transport, with mobility parallel to the [0001] direction significantly lower relative to the in-plane [1120] mobility⁸⁻¹⁰. This anisotropy has been associated with scattering from BSFs qualitatively, although no quantitative model exists. In this letter, we develop a theory of carrier scattering phenomena from BSFs and a quantitative estimate of the transport anisotropy is presented with comparison to experimental data.

Stacking faults (SF) are 2D structural defects associated with heteroepitaxial growth on lattice-mismatched substrates. Most prevalent SFs in wurtzite (WZ) nitrides is of the I_1 -type requiring lowest energy of formation¹¹. Scattering-contrast transmission microscope (TEM) imaging revealed⁵ that the SFs in GaN are primarily of the I_1 -type which corresponds to a stacking sequence of (0001) basal plane $\dots ABABABCBCBC \dots$. A BSF can be thought as a thin zincblende (ZB) layer (up to three monolayers thick) perfectly inserted in the WZ matrix without broken bonds as shown in Fig.1a). The built-in polarization difference between ZB and WZ structures will result in bound sheet charges $\pm\sigma_\pi$ at each

interface of the BSF layer. Consequently, the band edge will bend near the BSF. Fig.1b) shows a typical conduction band diagram around a BSF for a n-doped GaN film along with the charges that are formed in the direction perpendicular to the BSF plane. The bending of conduction band edge inside the BSF is due the electric field resulting from the polarization bound charge, whereas, bands bend outside the BSF due to the accumulation and depletion of mobile charges. We approximate the accumulation charge as a sheet charge of density n_s at the centroid (t) of the charge distribution, i.e. $\rho_\pi(x) = en_s\delta(x - x_0)$, where $x_0 = d + t$, d being the width of a BSF and e is the electron charge. If x_d is the width of the depletion region, charge neutrality requires $n_s = x_d N_d$, where N_d is the donor density. Energy conservation across the BSF leads to the relation

$$\frac{eN_d x_d^2}{2\epsilon_s} + \frac{en_s t}{2\epsilon_s} = \left(\frac{e\sigma_\pi}{2\epsilon_s} - \frac{en_s}{2\epsilon_s} \right) d, \quad (1)$$

where, ϵ_s is the permittivity of the semiconductor. In the limit $x_d \gg (t, d)$, the depletion length is $x_d \simeq \sqrt{\sigma_\pi d / N_d}$.

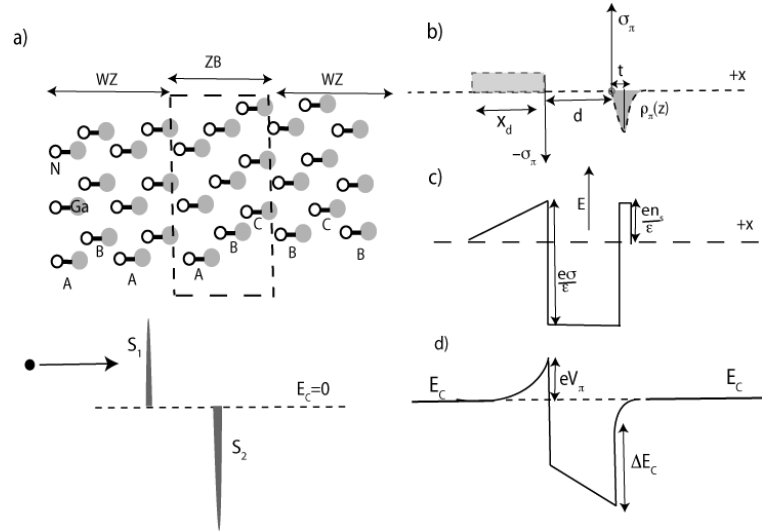


FIG. 1. a) structure of basal stacking faults, b) charges across the basal stacking fault, c) schematic diagram of electric field, d) conduction band diagram including band-offset, e) delta-function model of barrier and QW.

a) akonar@nd.edu

68 The depletion width x_d increases with decreasing donor
69 density and there exists a critical donor density N_d^{cr} for
70 which, x_d becomes equal to the distance between two
71 stacking faults. As a result the whole channel is depleted,
72 and conduction ceases along the x direction. The critical
73 donor density above which onset of conduction along x
74 direction occurs is given by $N_d^{cr} \geq \sigma_\pi dn_{SF}^2$. For a typical
75 fault density $n_{SF} = 10^5/\text{cm}$ and $d = 0.8 \text{ nm}$ for GaN¹²,
76 the critical doping density is $N_d^{cr} = 10^{16}/\text{cm}^3$. In the rest
77 of the paper, we will work in the regime where $N_d \gg N_d^{cr}$.

78
79 In addition to the polarization charges at interfaces,
80 the conduction band offset (ΔE_c) between ZB and WZ
81 structures leads to a quantum well (QW) in the fault re-
82 gion as shown in Fig.1b). For an applied bias, electrons
83 tunnel through the barrier (in the depletion region) and
84 QW (in the fault region) and then diffuse in the space
85 between two consecutive stacking faults. To model the
86 transmission coefficient of tunneling, we approximate the
87 barrier and the QW as two delta functions (as shown in
88 Fig.1e) of strengths $S_1 = eV_\pi x_d$ and $S_2 = (\Delta E_c + eV_\pi)d$;
89 where $V_\pi = \sigma_\pi d/2\epsilon_s$. The energy dependent coefficient of
90 transmission through a single delta function potential is
91 an analytically solvable problem¹³. If $T_{tr,1}(\epsilon)$ and $T_{tr,2}(\epsilon)$
92 are the transmission coefficient from the barrier and the
93 QW respectively, then the total coefficient of transmis-
94 sion across the BSF is given by $T_{tr}(\epsilon) = T_{tr,1}(\epsilon)T_{tr,2}(\epsilon)$:

$$T_{tr}(\epsilon) = \left[\frac{1}{1 + \frac{m^* S_1^2}{2\hbar^2 \epsilon}} \right] \times \left[\frac{1}{1 + \frac{m^* S_2^2}{2\hbar^2 \epsilon}} \right], \quad (2)$$

95 where, ϵ is the energy of the incoming electron and m^* is
96 the effective mass at the band edge. In SF-free structures,
97 the elemental current component along the x direction
98 for an electron with velocity v_k is given by $j_k^x = ev_k^x \delta f_k$;
99 where δf_k is the modification of equilibrium Fermi-Dirac
100 distribution caused by an applied electric field F_{appl} . In
101 the presence of SFs, a part (given by Eq. 2) of these
102 carriers is transmitted through the barrier and the QW
103 leading to an effective elemental current density $j_k^{eff} =$
104 $T_{tr}(\epsilon)j_k^x$. Then, the total current density in the presence
105 of SFs is given by

$$J_x = 2e \int \frac{d^3 k}{(2\pi)^3} T_{tr}(\epsilon) v_k^x \delta f_k, \quad (3)$$

106 where, v_k^x is the x component of electron group velocity
107 in the state $|\mathbf{r}, \mathbf{k}\rangle$ and the factor 2 takes spin degeneracy
108 into account. For a small applied electric field along
109 the x direction, under the relaxation time approximation
110 (RTA), $\delta f_k \approx (-\partial f_0/\partial \epsilon) \tau(k) v_k^x F_{appl}$, where, f_0 is the
111 equilibrium Fermi-Dirac distribution function and $\tau(k)$
112 is the momentum relaxation time due to scattering from
113 impurities, phonons etc present in the material. Inte-
114 grating Eq.3 over all k -space and defining conductivity
115 by the relation $J_x = \sigma(n, T) F_{appl}$, one obtains the car-
116 rier concentration (n) and temperature (T) dependent
117 conductivity in the presence of BSFs. The expression for

conductivity across the BSF is then given by

$$\sigma_{xx}(T, n) = \frac{3ne^2 \int d\epsilon \epsilon^{1/2} \cosh^{-2}(\epsilon/2k_B T) T_{tr}(\epsilon) \tau(\epsilon) (v_x^k)^2}{8\pi \int d\epsilon \epsilon^{3/2} \cosh^{-2}(\epsilon/2k_B T)}, \quad (4)$$

119 where T is the equilibrium temperature, k_B is Boltzmann
120 constant. Since the BSF does not break the periodic
121 symmetry in the y and z directions, inserting $T_{tr}(\epsilon) = 1$
122 for all energies, a similar expression can be obtained
123 for conductivity (σ_{yy}) along the y direction. For hole
124 transport, ΔE_c should be replaced by valence band
125 offset (ΔE_v) in the strength of delta function potential
126 S_2 , and a hole effective mass should be used instead of
127 the electron effective mass.

128
129 Equation (4) is the central finding of this work as
130 it allows us to calculate experimentally measurable
131 quantities such as conductivity and mobility in the
132 presence of BSFs. As an application of the formalism
133 constructed above we investigate charge transport in
134 p-type m -plane (1 $\bar{1}00$) GaN in the presence of BSFs, and
135 compare the results with previous reported experimental
136 data. Inclusions of different scattering mechanisms are
137 necessary to evaluate the energy dependent momentum
138 relaxation time $\tau(\epsilon)$ appearing in Eq.4. Due to the
139 high activation energy of acceptors (Mg for p-type
140 GaN has activation energy $\sim 174 \text{ meV}$ ⁸), a large
141 fraction of the dopants remain neutral even at room
142 temperature, acting as neutral impurity scatterers to
143 hole transport. The fact that a high doping density
144 is required to achieve appreciable hole concentrations
145 results in high density of neutral impurities (NI) making
146 neutral impurity scattering dominant even at room
147 temperature. Accounting for the zero-order phase
148 shift¹⁴, the momentum relaxation time of neutral
149 impurity scattering is $\tau_{NI}^{-1} = 20N\hbar a_0/m^*$; where N is
150 the density of neutral impurities and $a_0 = 4\pi\epsilon_s\hbar^2/m^*e^2$
151 is the effective Bohr radius. Momentum relaxation
152 time due to ionized impurity scattering (τ_{imp}) is
153 calculated following the method of Brooks-Herring
154 (BH)¹⁵. The fact that $\tau_{imp} \sim n_{imp}^{-1}$; where n_{imp} is the
155 density of ionized impurities, makes ionized impurity
156 scattering important at high carrier concentrations
157 (ionized dopant concentrations). For electron-optical
158 phonon momentum-relaxation time (τ_{ph}), only phonon
159 absorption has been considered due to the high optical
160 phonon energy ($E_{op} = 0.092 \text{ eV} \gg k_B T$) of GaN. The
161 resultant momentum-relaxation time is calculated using
162 Mathiessen's rule; i.e. $\tau(\epsilon)^{-1} = \tau_{NI}^{-1} + \tau_{imp}^{-1} + \tau_{ph}^{-1}$. For
163 numerical calculations, we assume the valence band
164 offset $\Delta E_v = 0.06 \text{ meV}$ ¹¹. The hole effective mass of GaN
165 is not well known and a wide range $m_h^* = 0.4 - 2.4m_0$
166 (m_0 is the rest mass of a bare electron) is found in
167 existing literature². In this work, we have assumed
168 $m_h^* \sim 1.8m_0$. Neutral impurity density is chosen to be
169 $N = 24 \times p$, where p is free hole concentration in GaN.
170 This choice is not ad hoc; measurements⁸ show that the
171 neutral impurity density $N = N_A - p \approx 20 - 25 \times p$ for

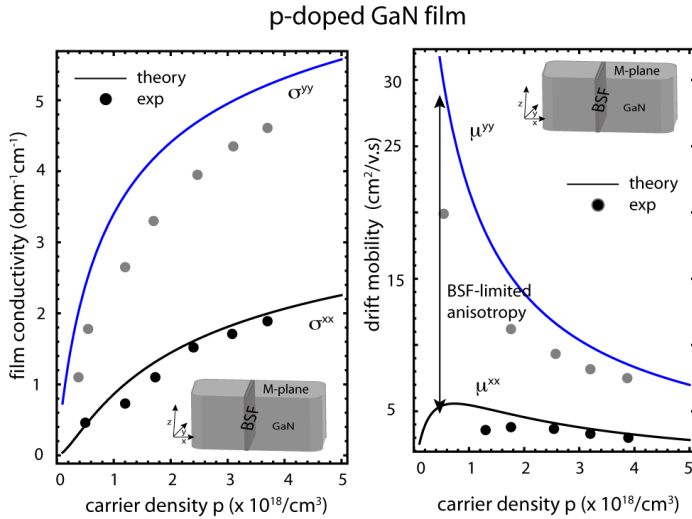


FIG. 2. a) hole conductivity as a function of hole density: anisotropy is due to BSF b) hole mobility as a function of hole density. solid lines are theoretical values and solid circles are experimental values from ref. 7.

172 a wide range of acceptor densities N_A .
173

174 Figure 2a) shows the calculated (solid lines) variation
175 of σ_{xx} (along the c -axis) and σ_{yy} (parallel to a axis) as a
176 function of hole density at room temperature juxtaposed
177 with experimental⁸ data (filled circles). It is apparent
178 from the figure that the presence of BSF causes an
179 appreciable reduction of σ_{xx} compared to σ_{yy} , resulting
180 in anisotropic hole transport. The corresponding hole
181 mobility $\mu_{ii} = \sigma_{ii}/pe$; $i = x, y$, is shown in Fig.2b). The
182 anisotropy in hole mobility increases with decreasing
183 hole density. This stems out from the fact that, in the
184 limit $p \rightarrow 0$, the depletion width increases ($x_d \sim N_A^{-1/2}$)
185 and one approaches the critical acceptor density limit
186 N_A^{cr} . As x_d increases, the strength of the barrier S_1
187 increases, and $T_{tr}(\epsilon) \rightarrow 0$. This results in vanishing μ_{xx}
188 (σ_{xx} ; see Fig.2).
189

190 We next investigate the electron transport in n-doped
191 samples in the presence of BSFs. Experiment⁸ shows
192 that electron mobility in m-plane GaN decreases with de-
193 creasing electron concentration. This phenomena is well
194 described by charged dislocation scattering as pointed
195 out by Weimann et. al¹⁶. The large lattice mismatch
196 between GaN and the substrate (for GaN on SiC, lattice
197 mismatch $\sim 2.9\%$) leads to high dislocation densities.
198 For m-plane GaN grown on foreign substrates,
199 TEM images reveal^{17,18} edge dislocation lines perpendic-
200 ular to the m-plane (along the $[1\bar{1}00]$ direction) with
201 non zero Burger's vector along $[0001]$ direction. Each
202 dislocation line acts as an acceptor-like trap with a line
203 charge density $\rho_L = e/a$, where a is the a -lattice con-
204 stant of GaN. The electrons moving in the perpendicular
205 plane to the dislocation line effectively feel a Coulomb

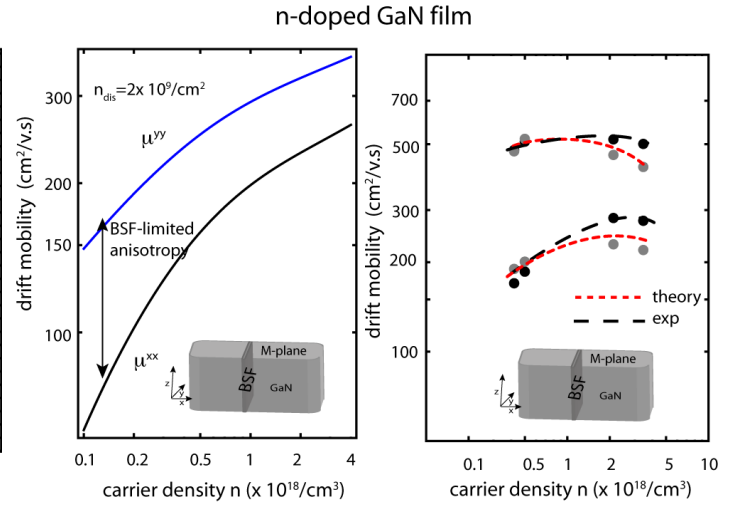


FIG. 3. a) electron mobility as a function of electron density, b) comparison between theoretical values (dotted line) and experimental values (dashed line) of electron mobility at different values of electron concentrations.

206 potential $V(r) = (\rho_L/2\pi\epsilon_s)K_0(r/L_D)$, where $K_0(\dots)$
207 is the zeroth order Bessel function of 2nd kind and
208 $L_D = \sqrt{k_B T \epsilon_s / e^2 n'}$ is the Debye screening length. Both
209 free electrons, and bound electrons are taken account in
210 the effective screening concentration (n') using Brook's¹⁹
211 formula $n' = 2n - n^2/N_D$; where n is the free carrier con-
212 centration. The momentum relaxation time (τ_{dis}) due
213 to dislocation lines has been calculated by several au-
214 thors for three^{16,20,21} and two-dimensional electron gas²²
215 in GaN. In the presence of BSFs, the x component of con-
216 ductivity at room temperature due to dislocation scatter-
217 ing can be calculated as

$$\sigma_{xx}^{dis} = \left(\frac{\epsilon_s}{e^2}\right)^2 \frac{3ne^2 a^2 (k_B T)^{3/2}}{4\pi\sqrt{m^*} n_{dis} L_D} \mathcal{I}(n, \Delta E_c), \quad (5)$$

218 where, n_{dis} is the dislocation density and $\mathcal{I}(n, \Delta E_c)$ is a
219 dimensionless integral. The complex nature of the of the
220 integral $\mathcal{I}(n, \Delta E_c)$ prevents an analytical evaluation and
221 one must rely on numerical techniques. For $\Delta E_c = 0.27$
222 eV¹¹, and in the non-degenerate limit, $\mathcal{I}(n, 0.27) \simeq 6$,
223 and $\mu_{xx} \sim \sqrt{n}$. Fig. 3a) shows the room temperature
224 drift mobility with electron density for dislocation den-
225 sity $n_{dis} = 2 \times 10^9/\text{cm}^2$. It not only captures the mobil-
226 ity anisotropy due to BSF, but also the mobility varia-
227 tion with carrier concentration; the behavior is similar to
228 those measured experimentally^{8,16}. For calculations, we
229 used $m_{xx}^* = m_{yy}^* = 0.22m_0$, and a resultant momentum
230 relaxation time $\tau^{-1} = \tau_{dis}^{-1} + \tau_{NI}^{-1} + \tau_{imp}^{-1} + \tau_{ph}^{-1}$ is consid-
231 ered. Unlike p-doped GaN, the unintentionally doped C
232 atoms serve as neutral impurities with a measured den-
233 sity $N \sim 5 \times 10^{16}/\text{cm}^2$ ⁸. Measurements of ref. 7 show free
234 electron concentration using Hall technique is lower than
235 actual dopant concentration in n-doped non-polar GaN
236 samples. The difference between the dopant concentra-
237 tion and the free electron concentration is attributed to
238

the acceptor traps associated with the dislocation lines. Moreover, the difference $(N_D - n) \sim n_{dis}$ varies from sample to sample indicating sample dependent density of dislocations. Assuming a single trap per a -lattice constant, the volume density of trapped charge is n_{dis}/a ; and a charge balance equation can be written as

$$n + \frac{n_{dis}}{a} = \frac{N_D}{1 + \frac{n}{2N_C} \exp(E_D/k_B T)}, \quad (6)$$

where, $N_C = 2(m^*k_B T/2\pi\hbar^2)^{3/2}$ is the effective density of states and E_D is the activation energy of the donor level. The screening effect on the donor activation energy is taken account by the empirical formula $E_D = E_{D0} - \alpha N_D^{1/3}$ ²³, where the screening parameter $\alpha = 2.1 \times 10^{-5}$ meV.cm and $E_{D0} = 28$ meV²³. Using Eq. 6 and values of N_D and n from ref. 7 calculated dislocation densities are found to be in the range of $n_{dis} \sim 1-10 \times 10^8$ /cm². Electron mobilities is determined using the calculated values of sample-dependent dislocation densities and compared to experimentally measured values as shown in Fig. 3b). At low carrier densities, theoretical values are in agreement with experimental data; but they differ at high carrier concentrations.

An important observation is that the anisotropy in electron and hole mobilities decreases with increasing carrier concentration. At higher carrier densities, transmission of carriers occupying higher energy states approaches unity ($T_{tr}(\epsilon) \rightarrow 1$) leading to $\mu_{xx} \sim \mu_{yy}$. The corresponding carrier density is $n_0(p_0) \simeq 1/3\pi^2(m^*\Delta E_{c(v)}d/\hbar^2)^3$ ($\sim 10^{19}$ /cm³), above which BSF-induced transport anisotropy vanishes in non-polar GaN. At high acceptor concentrations, the energy levels of impurity atoms overlaps to form impurity bands. While conduction through this impurity band is important at low temperatures, at room temperature impurity band does not form an efficient transport path²⁴ and its exclusion from our model is quite justified. Also, the comparison between theoretically calculated drift mobility and experimentally measured Hall mobility is meaningful as at room temperature, the Hall factor $r_H \sim 1$ ²³. Our work presented here can be improved in three ways; i) at low carrier densities x_d is large; assumption of the delta function barrier breaks down and one should solve the Schrodinger equation numerically to obtain exact transmission coefficient $T_{tr1}(\epsilon)$, and ii) at low doping levels (when x_d is large) or for high stacking fault density, carriers are confined in a quasi-two dimensional space rather than moving in three dimensions. Hence, one should use a two-dimensional analogue of Eq.4 for an exact evaluation of μ_{yy} , and iii) by incorporating the contributions of quasi-localized¹² electrons in the shallow state of the thin QW located in the fault region.

High-quality (low defect densities) non-polar GaN is

currently under development. It is apparent that with decreasing SF density, transport anisotropy will decrease and eventually vanishes for BSF free non-polar GaN films. The theory presented here is not only applicable to GaN, but to any semiconductor (including other members of the nitride family such as InN⁶ and AlN⁷) having BSFs with proper choice of material parameters. For example, the semiconductor zinc-oxide (ZnO) shows SFs similar to GaN with $\sigma_\pi = .057$ C/m² and the band offsets²⁵ are $\Delta E_c = 0.147$ eV and $\Delta E_v = 0.037$ eV.

In summary, we have presented a transport theory in semiconductors containing a large number of basal stacking faults. The theory is applied to understand the experimentally observed transport anisotropy in m-plane GaN and a reasonable agreement between theory and experiment is obtained. Two critical limits of carrier concentration are derived, one where transport across a basal stacking fault ceases and another, where the presence of basal stacking faults can be ignored in the context of charge transport.

The authors would like to acknowledge J. Verma, S. Ganguly (University of Notre Dame) for helpful discussions and National Science Foundation (NSF), Midwest Institute for Nanoelectronics Discovery (MIND) for the financial support for this work.

- ¹P. Waltereit *et al.* Nature **406**, 865 (2000).
- ²J. Piprek, *Nitride Semiconductor Devices: Principles and Simulations* (Wiley-VCH, Weinheim, 2007).
- ³C. Wood and D. Jena, *Polarization Effects in Semiconductors: From Ab Initio Theory to Device Applications* (Springer, NY, 2008).
- ⁴Y. Cai *et al.*, IEEE Electron Device Lett. **26**, 435 (2005).
- ⁵B. A. Haskell *et al.*, J. Electron. Mater. **34**, 357 (2005).
- ⁶C. Hsiao *et al.*, J. Appl. Phys. **107**, 073502 (2010).
- ⁷K. Ueno, A. Kobayashi, J. Ohta and H. Fujioka, Jpn. J. Appl. Phys. **49**, 060213 (2010).
- ⁸M. McLaurin, T. E. Mates, F. Wu and J. S. Speck, J. Appl. Phys. **100**, 063707 (2006).
- ⁹M. McLaurin, T. E. Mates, and J. S. Speck, Phys. Stat. Sol. (RRL), **1**, 110 (2007).
- ¹⁰K. H. Baik *et al.*, IEEE. Photon. Technol. Lett. **22**, 595 (2010).
- ¹¹C. Stampfl and C. G. Van de Walle, Phys. Rev. B. **24**, R15052 (1998).
- ¹²Y. T. Rebane, Y. G. Shreter and M. Albrecht, Phys. Stat. Sol. (a) **164**, 141 (1997).
- ¹³D. J. Griffiths, *Introduction to Quantum Mechanics* (Pearson Education Inc. Singapore, 2005).
- ¹⁴C. Erginsoy, Phys. Rev. **79**, 1013 (1950).
- ¹⁵H. Brooks, Phys. Rev. **83**, 879 (191).
- ¹⁶N. G. Weimann and L. F. Eastman, J. Appl. Phys. **83**, 3656 (1998).
- ¹⁷I. Lo *et al.*, Appl. Phys. Lett. **92**, 2020106 (2008).
- ¹⁸D. N. Zakharov and Z. Liliental-Webber, Phys. Rev. B. **71**, 235334 (2005).
- ¹⁹K. Seeger, *Semiconductor Physics: An Introduction*, 7th Ed. pp-173, (Springer, New York, 1999).
- ²⁰B. Pödör, Phys. Stat. Sol. **16**, K167 (1966).
- ²¹D. C. Look and J. R. Sizelove, Phys. Rev. Lett. **82**, 1237 (1998).
- ²²D. Jena, A. C. Gossard and U. K. Mishra, Appl. Phys. Lett. **76**, 1707 (2000).
- ²³D. C. Look *et al.*, Solid State. Comm. **102**, 297 (1997).
- ²⁴D. Lancefield and H. Eshghi, J. Phys.: Condens. Matter **13**, 8939 (2001).
- ²⁵Y. Yan *et al.*, Phys. Rev. B. **70**, 193206 (2004).